International Journal of Solids and Structures 102–103 (2016) 259–266

Contents lists available at ScienceDirect

International Journal of Solids and Structures

journal homepage: www.elsevier.com/locate/ijsolstr

Measuring the nonlocal effects of a micro/nanobeam by the shifts of resonant frequencies

Yin Zhang*, Ya-Pu Zhao

State Key Laboratory of Nonlinear Mechanics (LNM), Institute of Mechanics, Chinese Academy of Sciences, Beijing 100190, China

ARTICLE INFO

Article history:
Received 7 May 2016
Revised 21 September 2016
Available online 30 September 2016

Keywords:
Nonlocal effects
Micro/nanobeam
Resonant frequency
Inverse problem

ABSTRACT

A method of using the shifts of the beam resonant frequencies to determine the unknown parameters of nonlocal effects together with other effects such as surface elasticity, surface stress and residual stress is presented. The nonlocal effects are size-dependent, which only stand out when a specimen size diminishes. However, when the size of a specimen is small, other effects may also impact its mechanical properties and it is difficult to tell them apart. Unlike the static tests, the dynamic method presented in this study can differentiate various effects and thus determine the parameters. The parameters of different effects are solved as an inverse problem and the accuracy of the method is also demonstrated. So far, there are still no clear physical mechanisms to determine the parameters of nonlocal effects and different experiments yield different results. Because of the sensitivity to pre-existing defects, the mechanical properties of a small specimen may vary from one to another and the nonlocal effects can be disguised by other effects, which leads to different or even wrong interpretations on experimental data. With the capability of differentiating various effects, this study provides a more accurate and reliable method of determining the parameters of nonlocal effects, which should be of some help to the nonlocal theories.

1. Introduction

An extension of classical elasticity to a generalized continuum is given as follows (Aifantis, 2003)

$$(1-l_1^2\nabla^2)t_{ij}(x) = C_{ijkl}(1-l_2^2\nabla^2)\epsilon_{kl}(x), \quad (1)$$

where $t_{ij}(x)$ is the nonlocal stress at the reference point x and ϵ_{kl} is the (classical) strain (Eringen, 1983); $\nabla^2 = \partial^2/\partial x_1^2 + \partial^2/\partial x_2^2$ is the Laplacian operator and C_{ijkl} is the elastic modulus tensor. l_1 and l_2 are two characteristic lengths. When $l_1 = 0$ and $l_2 \neq 0$, i.e., that the stress gradient terms are gone, Eq. (1) is reduced to the strain gradient elasticity model (Aifantis, 2003; Mindlin and Eshel, 1968), which is also variously called Cosserat theory (Cosserat and Cosserat, 1909; Yang and Lakes, 1982), couple stress theory (Koiter, 1964; Mindlin and Tiersten, 1962), microstructure theory (Mindlin, 1964), micropolar theory (Eringen and Liebowitz, 1968), micromorphic theory (Forest, 2009) and microstrain theory (Forest and Sievert, 2006) though there are some kinematic differences among the above theories (Forest, 2009; Lakes, 1986). When $l_2 = 0$ and $l_1 \neq 0$, i.e., that the strain gradient terms are gone, Eq. (1) is reduced to the nonlocal elasticity model (Eringen, 1983). Both the strain gradient elasticity and nonlocal elasticity theories are the continuum approach representing a macroscopic approximation to a microscopic model, which admits discreteness, inhomogeneity and long-ranged forces (Fleck and Willis, 2015). The discreteness and inhomogeneity of a polycrystal nanobeam are shown in Fig. 1(a). Because an infinitesimal surface element can transmit both force and moment (Koiter, 1964), microrotation is balanced by such moment, which is also variously called couple stress (Mindlin, 1963), torque stress (Kröner, 1963) and stress moment (Adomeit and Kröner, 1967). Couple stress is related with the curvature, i.e., the second gradient of displacement (Mindlin, 1963). Therefore, a characteristic length (l_2) must be involved, which is also required by dimensional grounds. This length is a material property on which the influence of couple stress depends strongly (Mindlin, 1963) and is intimately related to the range of the interatomic forces (Kröner, 1963). In comparison, Eringen's (1983) nonlocal elasticity theory is much more straightforward to incorporate nonlocality by assuming that stress at a point depends not only on the strain at that point but also on strains at all other points of the body. In atomistic simulation, the above assumption can be translated as follows: the forces acting on an atom of a solid are due not only to the nearest neighbor atoms but also to all atoms in the solid (McFarland and Colton, 2005), which is another way of stating the long-ranged nature of interatomic forces. The long-ranged effect of interatomic forces is now embodied in the length of l_1.

* Corresponding author.
E-mail address: zhangyin@lnm.imech.ac.cn (Y. Zhang).

http://dx.doi.org/10.1016/j.ijsolstr.2016.09.034
0020-7683/

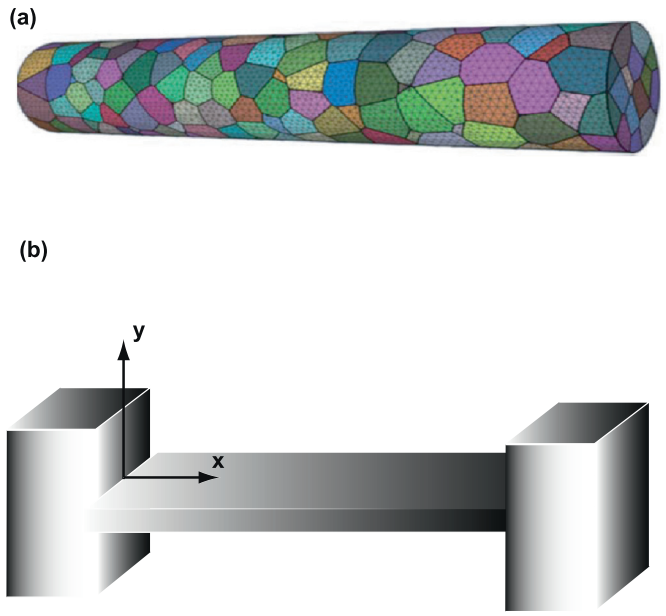

Fig. 1. (a) The schematic diagram of a nano-polycrystal beam. Due to the presence of the microstructure of grain and the small size of beam, the properties of inhomogeneity and long-ranged atomic interactions stand out, which leads to the nonlocal effects. (b) The schematic diagram of a clamped-clamped beam and its coordinate system.

Clearly, l_1 and l_2 are two critical length scales on which the nonlocal effects depend. The full utility of the nonlocal theories hinges on one's ability to determine these characteristic lengths (Abu-Al-Rub and Voyiadjis, 2004). However, how to determine these two lengths has been an important problem since the nonlocal theories were established. As commented by Yang and Lakes (1981), the nonlocal theories, which makes reference neither to underlying cause nor to structure, are purely phenomenological. The introduction of these lengths is based on "mathematical structure" (Aifantis and Willis, 2005), or say, dimensional analysis. The nonlocal theories themselves cannot identify these characteristic lengths (Koiter, 1964; Mindlin and Eshel, 1968). Although the provision of the actual values for l_1 or l_2 must rely on a clear recognition of physics (Aifantis and Willis, 2005) and such physical picture is not clear yet, there are still two methods to determine these characteristic lengths. One is to match the results predicted by the nonlocal theories with the experimental data. Unlike the classical elasticity theory, the nonlocal theories predicate that the bending and torsion rigidities, stress-strain relation, or say, (effective) Young's modulus and shear modulus are size-dependent and deviate from the classical values (Koiter, 1964), which is the very mechanism for experiment to determine those characteristic lengths. However, the torsion test of aluminum-epoxy composite (Gauthier and Jahsman, 1975), the bending tests of aluminum alloy (Schijve, 1966), aluminum and low-carbon steel (Ellis and Smith, 1966) all failed to detect the nonlocal effects of strain gradient elasticity. The failure reason was thought to be the measurement accuracy by Kakunai et al. (1985) and by adopting a measurement method with much higher accuracy, their bending tests of high purity aluminum show that l_2 is one fifth of the grain size. As discussed later, besides the measurement accuracy, there are more reasons for the failure of detecting the nonlocal effects. The other method is to match the results predicted by the nonlocal theories of elastic continuum governed by differential equations with those by the discrete atomistic simulation or lattice dynamics governed by difference equation. For example, Eringen and Liebowitz (1968) found $l_1 = 0.39a$ (a: lattice parameter) by matching the dispersion relation predicted by the nonlocal elasticity theory with that by Born-Kármán model of lattice dynamics. By matching the buckling strains predicted by the nonlocal elasticity theory and by the atomistic simulation, Zhang et al. (2005) found $l_1 = 0.82a$. Similarly, by matching the constitutive relations derived by the continuum strain gradient elasticity theory and by the discrete atomistic model, Wang and Hu (2005) found $l_2 = a/\sqrt{12}$. However, besides the expensive and time-consuming computation, the atomistic simulation suffers two major drawbacks, which make its use of determining the characteristic lengths less accurate or even inapplicable. Firstly, (most) discrete atomistic simulations inevitably employ "an idealised version of underlying physics" (Aifantis and Willis, 2005). Secondly, because the pre-existing defects can affect the nonlocal effects (Maranganti and Sharma, 2007a; 2007b), for an atomistic simulation to start, the defects must be specified, which is an impossible scenario for most real applications. Furthermore, nonlocal effects can be clouded by other effects and it is difficult to differentiate various effects. McFarland and Colton (2005) used the bending test of a polypropylene microcantilever to determine the nonlocal effects due to couple stress by monitoring the change of bending rigidity. They outlined three possible error sources for the measurement of the polymer beam bending rigidity: molecular orientation-induced anisotropy, residual stress and the formation of "skin" on the beam one or both sides due to the cooling asymmetry during the molding process (McFarland and Colton, 2005). The above error sources can be significant and thus dramatically influence how we interpret the experimental data and thus bending rigidity. In the above experiments (Ellis and Smith, 1966; Gauthier and Jahsman, 1975; Kakunai et al., 1985; McFarland and Colton, 2005; Schijve, 1966) and simulations (Eringen, 1983; Wang and Hu, 2005; Zhang et al., 2005), there is only one unknown parameter: l_1 or l_2. By matching the result of nonlocal theories with that of experiment or simulation, there is an one-to-one relation, which can uniquely determine l_1 or l_2. If the number of unknown parameters is more than one, such one-to-one relation does not exist. For example, the nonlocal effect due to the strain gradient elasticity theory (l_2) concludes that "smaller is stiffer" (Ellis and Smith, 1966; Gauthier and Jahsman, 1975; Kakunai et al., 1985; McFarland and Colton, 2005; Schijve, 1966). In contrast, the nonlocal effect due to the nonlocal elasticity theory says the opposite: "smaller is more compliant" (Zhang et al., 2005). Therefore, there is such possibility that in the static bending or torsion tests, these two competing nonlocal effects can cause no change in bending or torsion rigidity and from the experimental data, we have to conclude wrongfully that there is no nonlocal effect. Perkins and Thompson (1973) torsion tests of polyvinyl chloride foam material show that majority of experimental data follow the trend of "smaller is stiffer" predicted by the couple stress theory, but the opposite trend is also observed. At the same time, the scattering of their experimental data is also noticed. Similarly, Yang and Lakes (1982) bending tests of human bones conclude that l_2 in each specimen is different and its distribution ranges from 0.16 mm to 0.84 mm though the unit cell diameter of osteon keeps unchanged as 0.25 mm. In all of the above experiments (Ellis and Smith, 1966; Gauthier and Jahsman, 1975; Kakunai et al., 1985; McFarland and Colton, 2005; Perkins and Thompson, 1973; Schijve, 1966; Yang and Lakes, 1981), there are multiple specimens are used to obtain l_2 by curve-fitting. There is a potential problem of using multiple specimens to determine the characteristic lengths for one material. A localized defect can have an impact on the overall mechanical properties of a specimen (Murphy and Zhang, 2000; Wu and Wei, 2013). Furthermore, as the size of a specimen diminishes, its nonlocal effects (Maranganti and Sharma, 2007a; 2007b) and mechanical properties become more sensitive to pre-existing defects. It is not uncommon that reproducible re-

sults cannot be obtained for some nanomechanical sensors because of the device-to-device variations (Boisen, 2009). A vivid example is the significant variations of the "identical" microcantilevers in their higher modes vibrations as observed by Reed et al. (2009). At micron or nanometer scale, to extract the characteristic lengths from multiple specimens for a material can be erroneous because the characteristic lengths may vary from one to another due to the presence of defects.

In this study, a method of extracting the characteristic lengths from one specimen is presented, which is to use the shifts of resonant frequencies as the working mechanism. Because the difference between the results predicted by the classical and nonlocal theories are very small, static tests require very high measurement accuracy in order to detect the nonlocal effects (Kakunai et al., 1985). In comparison, the resonant frequencies of a small-scaled specimen are very large and therefore, a tiny shift of the resonant frequencies is still absolutely large enough to be readily detected and accurately measured. In that sense, this study provides a more reliable and accurate method than the static test to determine the nonlocal effects. Furthermore, the static tests are incapable of differentiating the effects of the strain gradient elasticity, nonlocal elasticity, surface elasticity surface stress and residual stress. The hallmark of the method presented here is that it can differentiate some of the effects, which makes it more accurate to detect the nonlocal effects. The verification of the results predicted by the nonlocal theories and calibration of the characteristic lengths are indispensable for applicability and justification of the nonlocal theories (Arash and Wang, 2012). Although some works on determining the characteristic lengths are mentioned above, the work on the evaluation of the characteristic lengths is quite few and certainly no clear consensus exists (Maranganti and Sharma, 2007a). With the higher accuracy and capability of differentiating various effects, besides determining the characteristic lengths, the method presented in this study also provides an effective approach of calibrating micro/nanomechanical device.

2. Model development

The equilibrium as given by the linear nonlocal elasticity theory is expressed by the following set of equations (Eringen and Liebowitz, 1968)

$$t_{ij,j} = 0, \tag{2}$$

$$t_{ij}(x) = \int_V \alpha(|x' - x|, \tau_o)\sigma_{ij}(x')dV(x'), \tag{3}$$

$$\sigma_{ij}(x') = C_{ijkl}\epsilon_{kl}, \tag{4}$$

$$\epsilon_{ij}(x') = \frac{1}{2}[u_{i,j}(x') + u_{j,i}(x')], \tag{5}$$

where $t_{ij}(x)$ is the nonlocal stress at the reference point x; σ_{ij} and ϵ_{ij} are the classical (local) stress and strain at any point x' in the elastic body; C_{ijkl} is the elastic modulus tensor and u_i is the displacement vector and $u_{i,j} = \partial u_i/\partial x_j$; V is the volume of elastic body. The kernel $\alpha(|x' - x|, \tau_o)$ is called nonlocal modulus (Eringen and Liebowitz, 1968), which can be seen as a correlation function. $|x' - x|$ is the Euclid norm denoting the distance; τ_o is a (dimensionless) constant, which in essence indicates the nonlocal effect and as $\tau_o \to 0$, $\alpha(|x' - x|, \tau_o) = \delta(|x' - x|)$ (δ is the Dirac delta function), which recovers the classical (local) elasticity theory. Again, the above equation set indicates that the real nonlocal stress $t_{ij}(x)$ depends on the strains at not only the reference point x but also all other points of the body (Eringen, 1983). The above equation set consists of a complex constitutive relation of integro-differential equations. As for a two-dimensional nonlocal modulus of α, the equation set of Eqs. (2)–(5) can be written approximately as follows (Eringen, 1983)

$$(1 - \tau_o^2 l^2 \nabla^2)t_{ij}(x) = (1 - e_o^2 a^2 \nabla^2)t_{ij}(x) = \sigma_{ij}(x) = C_{ijkl}\epsilon_{kl}(x), \tag{6}$$

where $\nabla^2 = \partial^2/\partial x_1^2 + \partial^2/\partial x_2^2$ is the Laplacian operator; l is an external characteristic length (e.g., crack length, wavelength) (Eringen, 1983); a is the elastic body internal length such as lattice parameter or grain size. e_o is a constant to be determined for each material. Clearly, we have $\tau_o l = e_o a$. In real applications, owing to the difficulty of determining a, many researchers have adopted $e_o a$ as a single parameter. Compared with Eq. (1), $e_o a$ corresponds to l_1. For an one dimensional Euler-Bernoulli beam, Eq. (6) is now written as follows (Arash and Wang, 2012; Xu, 2006; Zhang et al., 2009; 2010)

$$t_x - (e_o a)^2 \frac{\partial^2 t_x}{\partial x^2} = E^* \epsilon_x, \tag{7}$$

where t_x and ϵ_x are the axial normal stress and strain, respectively. E^* is the (unknown) effective Young's modulus. For a micro/nanometer scaled structure, a surface layer may form and the whole structure is like a composite one (He and Lilley, 2008; Zhang et al., 2013) and the presence of strain gradient in bending also effectively changes the beam bending rigidity (Kong et al., 2008; 2009). As a result, the beam effective Young's modulus can be different from a macroscopic one.

For an Euler-Bernoulli beam, the shear force S and bending moment M are related by the following equation

$$S = \frac{\partial M}{\partial x}. \tag{8}$$

With the presence of an axial force, F, the governing equation of a transversely vibrating Euler-Bernoulli beam is as follows (Xu, 2006)

$$\frac{\partial S}{\partial x} = -p - F\frac{\partial^2 w}{\partial x^2} + m\frac{\partial^2 w}{\partial t^2}, \tag{9}$$

where w and p are the transverse displacement and load per unit length, respectively. m is the mass per unit length and $m = \rho A$ (ρ: density and A: cross section area); t is time. By substituting Eq. (8) into Eq. (9), the following equation is derived

$$\frac{\partial^2 M}{\partial x^2} = -p - F\frac{\partial^2 w}{\partial x^2} + m\frac{\partial^2 w}{\partial t^2}. \tag{10}$$

Multiplying by y on both sides of Eq. (7) and integrating over the beam cross section, we have

$$\int_A y t_x dA - (e_o a)^2 \int_A \frac{\partial^2 t_x}{\partial x^2} dA = \int_A E^* y \epsilon_x dA. \tag{11}$$

By definition, the bending moment M is given as follows

$$M = \int_A y t_x dA. \tag{12}$$

For the small deflection of Euler-Bernoulli beam, we have

$$\epsilon_x = -y\frac{\partial^2 w}{\partial x^2}. \tag{13}$$

In conjunction with Eqs. (12) and (13), Eq. (11) is now written as the following

$$M - (e_o a)^2 \frac{\partial^2 M}{\partial x^2} = -E^* I \frac{\partial^2 w}{\partial x^2}, \tag{14}$$

where $I = \int_A y \epsilon_x dA$ is the area moment of inertia. Differentiating both sides of the above equation with respect to x twice leads to the following equation

$$\frac{\partial^2 M}{\partial x^2} - (e_o a)^2 \frac{\partial^4 M}{\partial x^4} = -E^* I \frac{\partial^4 w}{\partial x^4}. \tag{15}$$

Substituting Eq. (10) into Eq. (15) leads to the following

$$p-(e_oa)^2\frac{\partial^2 p}{\partial x^2}=E^*I\frac{\partial^4 w}{\partial x^4}-F\left[\frac{\partial^2 w}{\partial x^2}-(e_oa)^2\frac{\partial^4 w}{\partial x^4}\right]+m\left[\frac{\partial^2 w}{\partial t^2}-(e_oa)^2\frac{\partial^4 w}{\partial x^2\partial t^2}\right]. \tag{16}$$

When $p=\partial^2 p/\partial x^2=0$ and for statics, i.e., all time-related terms are gone, Eq. (16) becomes the following governing equation to study the nonlocal buckling (Zhang et al., 2009)

$$E^*I\frac{\partial^4 w}{\partial x^4}-F\left[\frac{\partial^2 w}{\partial x^2}-(e_oa)^2\frac{\partial^4 w}{\partial x^4}\right]=0. \tag{17}$$

In Eq. (16), the presence of p and $(e_oa)^2\partial^2 p/\partial x^2$ only influences the equilibrium position and the beam resonant frequencies do not change as these two terms vary. For simplicity, we set $p=\partial^2 p/\partial x^2=0$ and therefore, Eq. (16) becomes the following

$$E^*I\frac{\partial^4 w}{\partial x^4}-F\left[\frac{\partial^2 w}{\partial x^2}-(e_oa)^2\frac{\partial^4 w}{\partial x^4}\right]+m\left[\frac{\partial^2 w}{\partial t^2}-(e_oa)^2\frac{\partial^4 w}{\partial x^2\partial t^2}\right]=0. \tag{18}$$

In the vibration of a micro/nanobeam, there are three unknown parameters: E^*I, F and e_oa. For a given material, a is known as an intrinsic length, but e_o is an unknown fitting constant. Besides the applied axial load, there are two major sources contributing to F: surface stress (Altenbach and Eremeyev, 2011; He and Lilley, 2008; Karabalin et al., 2012; Zhang, 2013; Zhang et al., 2013; Zhang and Zhao, 2014) and residual stress (McFarland and Colton, 2005; Zhang and Zhao, 2015), which make F unknown in most micro/nanobeam applications. For the convenience of statement, we let $E^*I=EI+\Delta$. Here E is the Young's modulus of a macroscopic beam and EI is thus a known quantity. However, Δ here is unknown. Physically, Δ is the bending stiffness variation from that predicted by the classical theory. There are two major mechanisms causing Δ. One is surface elasticity (He and Lilley, 2008; Zhang et al., 2013) and the other is the another nonlocal effect as described by the strain gradient elasticity or couple stress theory (Kong et al., 2008; 2009). These two mechanisms are expressed as follows

$$\Delta=\Delta_1+\Delta_2,\qquad \Delta_1=\begin{cases}C_sh^2\left(\frac{1}{2}b+\frac{1}{6}h\right), & (rectangular),\\ \frac{\pi}{8}C_sD^3, & (circular),\end{cases}\qquad \Delta_2=\mu Al_2^2, \tag{19}$$

where Δ_1 and Δ_2 are the bending stiffness due to the surface elasticity and couple stress effects, respectively. In Δ_1, C_s is the surface modulus with the unit of $N\cdot m^{-1}$; h and b are the thickness and width of a rectangular beam, and D is the diameter of a circular beam. As mentioned above, the formation of surface layer, which can have different elastic properties from a bulk one (Altenbach and Eremeyev, 2011), makes the whole structure a *defacto* composite material (He and Lilley, 2008; Zhang et al., 2013). In Δ_2, μ is shear modulus and for an isotropic material, $\mu=E/2(1+\nu)$ (ν is the Poisson ratio); A is the cross-section area; As discussed above, l_2 is an intrinsic material length characterizing the effect of couple stress (Kong et al., 2008; 2009) or more generally, the range of interatomic forces (Kröner, 1963). In the strain gradient elasticity theory, the strain energy is dependent on not only strain but also strain gradients (Amiot, 2013; Kong et al., 2008; 2009). The additional strain energy contribution by the strain gradient part contributes to the bending rigidity increment of Δ_2. Although the strain gradient elasticity theory can model the surface/interface effects (Amiot, 2013; Mindlin, 1972), the above modeling approach in essence is to divide the beam into two parts: the bulk and surface layers (Zhang et al., 2015). In the bulk layer, the strain gradient elasticity (Amiot, 2013; Kong et al., 2008; 2009) and nonlocal elasticity (Eringen, 1983; Zhang et al., 2005; 2009) theories apply; and the surface layer is governed by the surface elasticity theory (He and Lilley, 2008; Zhang et al., 2013; 2015).

The following dimensionless quantities are introduced

$$W=\frac{w}{L},\quad \xi=\frac{x}{L},\quad \tau=\sqrt{\frac{EI}{mL^4}}t, \tag{20}$$

where L is the beam length. Eq. (18) is now nondimensionalized and re-arranged as the following

$$(1+\Lambda_1+\Lambda_2\Lambda_3)\frac{\partial^4 W}{\partial\xi^4}-\Lambda_2\frac{\partial^2 W}{\partial\xi^2}+\frac{\partial^2 W}{\partial\tau^2}-\Lambda_3\frac{\partial^4 W}{\partial\xi^2\partial\tau^2}=0. \tag{21}$$

Here the dimensionless Λ_1, Λ_2 and Λ_3 are defined as

$$\Lambda_1=\frac{\Delta}{EI},\quad \Lambda_2=\frac{FL^2}{EI},\quad \Lambda_3=\left(\frac{e_oa}{L}\right)^2, \tag{22}$$

Physically, Λ_1 indicates the dimensionless bending stiffness variation from the classical one; Λ_2 is the dimensionless axial load and Λ_3 is the square of two lengths ratio. Clearly, $\Lambda_3\geq 0$. Λ_1 and Λ_2 can be either positive or negative or zero. Positive/negative Λ_2 indicates that the axial force is tension/compression. Eq. (19) is now nondimensionalized as follows

$$\Lambda_1=\Lambda_{11}+\Lambda_{12},\quad \Lambda_{11}=\begin{cases}\frac{C_s}{E^*}\left(\frac{6}{h}+\frac{2}{b}\right), & (rectangular),\\ \frac{8C_s}{E^*D}, & (circular),\end{cases}$$

$$\Lambda_{12}=\frac{\mu Al_2^2}{E^*I}=\begin{cases}\frac{6l_2^2}{(1+\nu)h^2}, & (rectangular),\\ \frac{8l_2^2}{(1+\nu)D^2}, & (circular).\end{cases} \tag{23}$$

By assuming $W(\xi,\tau)=Y(\xi)e^{i\omega\tau}$ (ω: the dimensionless resonant frequency), Eq. (21) becomes the following

$$(1+\Lambda_1+\Lambda_2\Lambda_3)\frac{\partial^4 Y}{\partial\xi^4}-(\Lambda_2-\Lambda_3\omega^2)\frac{\partial^2 Y}{\partial\xi^2}-\omega^2 Y=0. \tag{24}$$

The corresponding characteristic equation is as follows

$$(1+\Lambda_1+\Lambda_2\Lambda_3)\lambda^4-(\Lambda_2-\Lambda_3\omega^2)\lambda^2-\omega^2=0, \tag{25}$$

which leads to the following two solutions

$$\lambda_1^2=\frac{\Lambda_2-\Lambda_3\omega^2+\sqrt{(\Lambda_2-\Lambda_3\omega^2)^2+4(1+\Lambda_1+\Lambda_2\Lambda_3)\omega^2}}{2(1+\Lambda_1+\Lambda_2\Lambda_3)},$$

$$\lambda_2^2=\frac{\Lambda_2-\Lambda_3\omega^2-\sqrt{(\Lambda_2-\Lambda_3\omega^2)^2+4(1+\Lambda_1+\Lambda_2\Lambda_3)\omega^2}}{2(1+\Lambda_1+\Lambda_2\Lambda_3)}. \tag{26}$$

As defined in Eq. (22), the dimensionless axial force of Λ_2 can be either a large or small quantity. However, we should point out that Eq. (21) is a linear equation. When Λ_2 reaches a critical negative value, the beam buckles and enters the post-buckling regime, which requires nonlinear analysis. For a hinged-hinged beam, the buckling load is $\Lambda_2=-\pi^2$; for a clamped-clamped beams, the buckling load is $\Lambda_2=-4\pi^2$ (Chajes, 1974). For Eq. (21) to be valid, Λ_2 is required to be larger than the buckling load. On the other hand, as seen in Eqs. (22) and (23), Λ_1 and Λ_3 are size-dependent; their effects only stand out when the beam characteristic lengths (L, b, h, D) are small. Λ_1 and Λ_3 are (very) small quantities, which ensures that $1+\Lambda_1+\Lambda_2\Lambda_3>0$. Therefore, $\lambda_1^2>0$ and $\lambda_2^2<0$. We define β_1 and β_2 as follows

$$\beta_1(\Lambda_1,\Lambda_2,\Lambda_3,\omega)=\sqrt{\lambda_1^2},\qquad \beta_2(\Lambda_1,\Lambda_2,\Lambda_3,\omega)=\sqrt{-\lambda_2^2}. \tag{27}$$

$Y(\xi)$ has the following solution form

$$Y(\xi) = C_1\cosh(\beta_1\xi) + C_2\sinh(\beta_1\xi) + C_3\cos(\beta_2\xi) + C_4\sin(\beta_2\xi), \tag{28}$$

where C_is ($i = 1$ to 4) are four unknown constants. The beam coordinate system is shown in Fig. 1(b) and the following four boundary conditions hold for a hinged-hinged beam

$$Y(0) = 0, \quad Y(1) = 0, \quad \frac{d^2Y}{d\xi^2}(0) = 0, \quad \frac{d^2Y}{d\xi^2}(1) = 0. \tag{29}$$

With the four boundary conditions of Eq. (29), Eq. (28) formulates an eigenvalue problem, which leads to the determination of the resonant frequency of ω. The resonant frequency of a hinged-hinged beam can be analytically derived as follows

$$\omega_n = n\pi\sqrt{\frac{\Lambda_2 + n^2\pi^2(1 + \Lambda_1 + \Lambda_2\Lambda_3)}{1 + n^2\pi^2\Lambda_3}}, \tag{30}$$

where ω_n is the nth resonant frequency (n is a positive integer). When $\Lambda_1 = \Lambda_2 = \Lambda_3 = 0$, Eq. (30) recovers the classical result of $\omega_n = n^2\pi^2$ (Chang and Craig, 1969). When $\Lambda_1 = \Lambda_2 = 0$, Eq. (30) becomes $\omega_n = n^2\pi^2/\sqrt{1 + n^2\pi^2\Lambda_3}$, which is the one derived by Zhang et al. (2010) for the nonlocal vibration. When $\Lambda_1 = \Lambda_3 = 0$, Eq. (30) becomes $\omega_n = n\pi\sqrt{\Lambda_2 + n^2\pi^2}$; and $\omega_1 = 0$ when $\Lambda_2 = -\pi^2$, which is the buckling load of a hinged-hinged beam (Chajes, 1974). As seen in Eq. (30), the nonlocal effect due to the strain gradient elasticity (as incorporated in the parameter of Λ_1) leads to a larger resonant frequency. In contrast, the nonlocal effect due to the nonlocal elasticity (as incorporated in the parameter of Λ_3) leads to a smaller resonant frequency.

For a clamped-clamped beam, the boundary conditions are the following four

$$Y(0) = 0, \quad Y(1) = 0, \quad \frac{dY}{d\xi}(0) = 0, \quad \frac{dY}{d\xi}(1) = 0. \tag{31}$$

Again, Eq. (28) with the four boundary conditions of Eq. (31) forms an eigenvalue problem for ω_n. Instead of an analytical solution, now the eigenvalue of ω_n has to be obtained by solving the following transcendental equation

$$2\beta_1\beta_2[1 - \cosh(\beta_1)\cos(\beta_2)] + (\beta_2^2 - \beta_1^2)\sinh(\beta_1)\sin(\beta_2) = 0 \tag{32}$$

3. Results and discussion

In order to calculate the eigenvalue of resonant frequency ω_n (e.g., Eq. (30) or (32)), the parameters of Λ_1, Λ_2 and Λ_3 must be supplied. Once Λ_1, Λ_2 and Λ_3 are given, ω_ns are uniquely determined as seen in Eq. (30). In most studies (Kong et al., 2008; 2009; Xu, 2006; Zhang et al., 2010; 2009), those parameters are given and varied to see how ω_n changes with them, which is the formulation of a forward/direct problem. However, in a real application, ω_ns are known/measured quantities and those parameters are unknowns. Now, an inverse problem arises: how to use the resonant frequencies to determine the bending stiffness variation, axial load and nonlocal elasticity effects?

In our case, there are three unknowns: Λ_1, Λ_2 and Λ_3. In order to present a graphic illustration and explain the mechanisms on how the inverse problem can be solved, we firstly present an example of two-unknown case and then solve the three-unknown case. Once again, when $\Lambda_1 = \Lambda_2 = \Lambda_3 = 0$, $\omega_n = n^2\pi^2$ as given by Eq. (30) for a hinged-hinged beam. We define the following quantities

$$\omega_1^o = \pi^2, \quad \omega_2^o = 4\pi^2, \quad \omega_3^o = 9\pi^2. \tag{33}$$

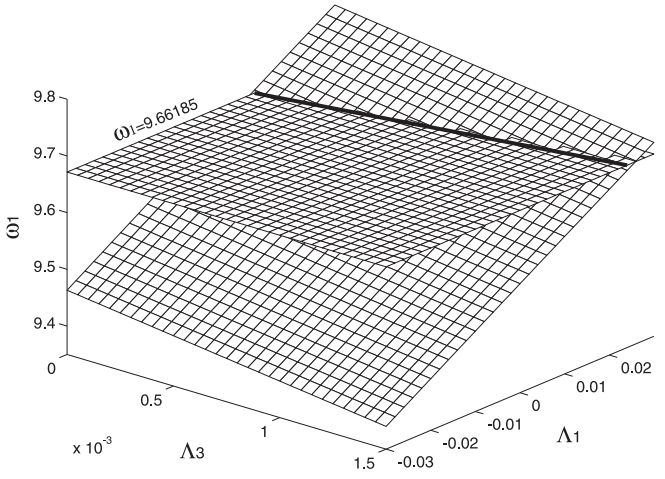

Fig. 2. The variation of the first resonant frequency (ω_1) as a function of Λ_1 and Λ_3. The level plane is the one with the constant of $\omega_1 = 9.66185$. The intersection of the two planes is marked with a solid line. Here $\Lambda_2 = -0.5$ is fixed.

Physically, ω_1^o, ω_2^o and ω_3^o are the first, second and third resonant frequencies predicted by the classical theory with zero bending stiffness variation, axial load and nonlocal elasticity effects. When Λ_1, Λ_2 and Λ_3 are given as follows

$$\Lambda_1 = 10^{-2}, \quad \Lambda_2 = -0.5, \quad \Lambda_3 = 10^{-4}, \tag{34}$$

the corresponding resonant frequencies change as the followings

$$\omega_1 = 9.66185 = 0.97895\pi^2, \quad \omega_2 = 39.34719 = 3.9867\pi^2,$$
$$\omega_3 = 88.6254 = 8.97963\pi^2. \tag{35}$$

Compared with the ω_n^os in Eq. (33), all of the three resonant frequencies become smaller. Here the axial load $\Lambda_2 = -0.5$ is moderately small, which is about 5% of the beam buckling load. As a demonstration example, suppose that $\Lambda_2 = -0.5$ is a known quantity, Λ_1 and Λ_3 are unknown. In Fig. 2, the variation of the first resonant frequency (ω_1) as a function of Λ_1 and Λ_3 is presented. ω_1 increases as Λ_1 increases. The reason for this is simple: larger bending stiffness results in larger resonant frequency. In contrast, ω_1 decreases as Λ_3 increases, which means that the nonlocal elasticity effect of Λ_3 reduces the system overall stiffness (Zhang et al., 2010; 2009). The level plane is the one with the constant of $\omega_1 = 9.66185$. The intersection of the two planes is marked with a solid line. Mathematically, this intersection line indicates that there are infinite combinations of Λ_1 and Λ_3, which result in the same first resonant frequency of $\omega_1 = 9.66185$. Therefore, the information of one resonant frequency is not sufficient to determine the two parameters. Similarly, in Fig. 3, the variation of the second resonant frequency (ω_2) as a function of Λ_1 and Λ_3 is also presented. Now the level plane is the one with the constant of $\omega_2 = 39.34719$. The intersection of the two planes is marked with a dashed line. Again, the same scenario is encountered: there are infinite combinations of Λ_1 and Λ_3 which result in the same second resonant frequency of $\omega_2 = 39.34719$. When the two lines obtained in Figs. 2 and 3 are projected onto the $\Lambda_1 - \Lambda_3$ plane, as presented in Fig. 4, the two lines intersect and the intersection point is marked by a circle, which exactly corresponds to (Λ_1, Λ_3) = (1×10^{-2}, 1×10^{-4}). Now the inverse problem of using two resonant frequencies (ω_1, ω_2) to determine two parameters (Λ_1, Λ_3) is solved. Inverse problems are often not well-posed problems and quite some inverse problems are unsolvable because of the lack of information (Anger, 1990; Gladwell, 2004). Here ω_ns are the information we can obtain from an experiment and for a continuous system, there are infinite ω_ns though in our case only two resonant frequencies are required. Besides the sufficient informa-

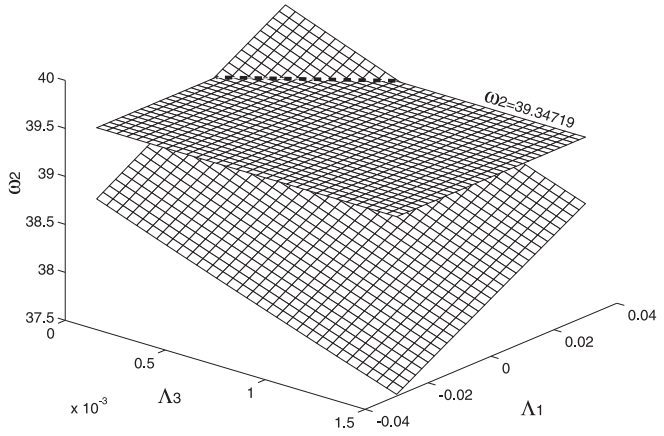

Fig. 3. The variation of the second resonant frequency (ω_2) as a function of Λ_1 and Λ_3. The level plane is the one with the constant of $\omega_2 = 39.34719$. The intersection of the two planes is marked with a dashed line. Here $\Lambda_2 = -0.5$ is fixed.

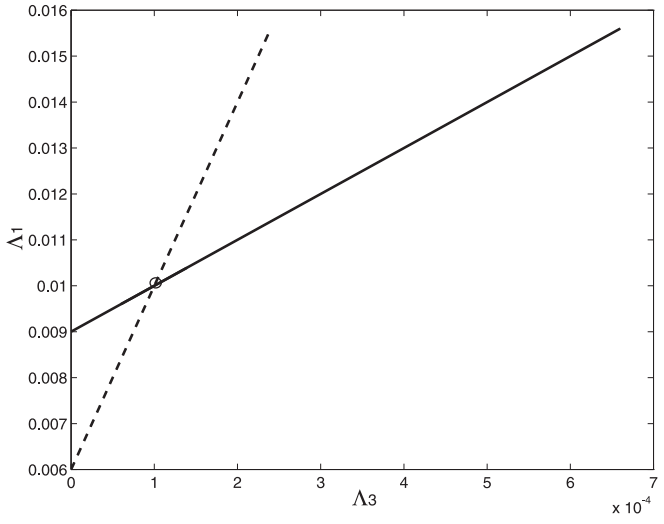

Fig. 4. The projections of the two intersection curves/lines obtained in Figs. 2 and 3 into the $\Lambda_1 - \Lambda_3$ plane. The intersection of the two curves is marked with a circle, which corresponds to (Λ_1, Λ_3)=$(1 \times 10^{-2}, 1 \times 10^{-4})$ exactly.

tion, there are two major physical mechanisms which make the inverse problem solvable. One is that for one resonant frequency, different parameter has different impact. This mechanism is seen in Eq. (30) that resonant frequency (ω_n) is a function of Λ_1, Λ_2 and Λ_3 and their impacts are different. This mechanism is also reflected in Figs. 2 and 3 that the slopes of resonant frequency (ω_1 or ω_2) planes along the Λ_1 and Λ_3 axes are significantly different. The other mechanism is that the impacts of the given parameters are different for different resonant frequencies. For example, the resonant frequencies of lower modes are much more sensitive to an axial load than those of higher modes (Zhang et al., 2013). In contrast, the nonlocal effects stand out more at higher modes. The size-dependent nonlocal effects are actually determined by three sizes: the unit cell size, the specimen size and the wavelength of variation of the applied mechanical field (Dillard et al., 2006). At the higher modes, the wavelength is shorter and the nonlocal effects are thus more prominent, which may be one of reasons for Reed et al. (2009) experimental observation that the variations of "identical" cantilevers in their higher modes are much more significant. This second mechanisms is also reflected in Fig. 4: the two lines are with two different slopes, which leads to intersection.

To solve the three-unknown case, we define the following function by modifying Eq. (30) for the convenience of statement

$$\mathcal{F}_n(\Lambda_1, \Lambda_2, \Lambda_3, \omega_n) = n\pi\sqrt{\frac{\Lambda_2 + n^2\pi^2(1 + \Lambda_1 + \Lambda_2\Lambda_3)}{1 + n^2\pi^2\Lambda_3}} - \omega_n. \tag{36}$$

For the inverse problem, ω_ns are the given values as determined by an experiment; Λ_1, Λ_2 and Λ_3 are the unknowns to be determined. When the first three resonant frequencies are supplied by Eq. (35), the following equation set is obtained

$$\begin{cases} \mathcal{F}_1(\Lambda_1, \Lambda_2, \Lambda_3, \omega_1) = \pi\sqrt{\frac{\Lambda_2+\pi^2(1+\Lambda_1+\Lambda_2\Lambda_3)}{1+\pi^2\Lambda_3}} - 9.66185 \\ \qquad\qquad = 0, \\ \mathcal{F}_2(\Lambda_1, \Lambda_2, \Lambda_3, \omega_2) = 2\pi\sqrt{\frac{\Lambda_2+4\pi^2(1+\Lambda_1+\Lambda_2\Lambda_3)}{1+4\pi^2\Lambda_3}} - 39.34719 \\ \qquad\qquad = 0, \\ \mathcal{F}_3(\Lambda_1, \Lambda_2, \Lambda_3, \omega_3) = 3\pi\sqrt{\frac{\Lambda_2+9\pi^2(1+\Lambda_1+\Lambda_2\Lambda_3)}{1+9\pi^2\Lambda_3}} - 88.6254 \\ \qquad\qquad = 0. \end{cases} \tag{37}$$

Mathematically, there are three (nonlinear) equations for the three unknowns of Λ_1, Λ_2 and Λ_3, which can be solved by the Newton-Raphson method (Press et al., 1992). In this case, the three unknowns are solved exactly as $(\Lambda_1, \Lambda_2, \Lambda_3) = (1 \times 10^{-2}, -0.5, 1 \times 10^{-4})$. When the Newton-Raphson method is applied, the initial guessed values of Λ_1, Λ_2 and Λ_3 need to be supplied. One advantage of the above inverse problem formulation is that the solution is not sensitive to the initial guess at all. In the above case, the initial guess is arbitrarily given as $(\Lambda_1, \Lambda_2, \Lambda_3) = (2.6 \times 10^{-2}, -3.9, 2.15 \times 10^{-4})$. Once the three unknowns of Λ_1, Λ_2 and Λ_3 are solved, the nonlocal elasticity effect can be directly obtained from the value of Λ_3. However, as defined in Eq. (23), Λ_1 is the bending stiffness variation and we cannot tell apart the contributions by the surface elasticity and by the strain gradient elasticity effect. Similarly, Λ_2 indicates the axial load variation; the contributions by surface stress and residual stress cannot be differentiated, either.

For a clamped-clamped beam, to solve the inverse problem, we need to modify some definitions for the convenience of statement. Firstly, the definitions of β_is of Eq. (27) are modified as follows

$$\beta_{1,n}(\Lambda_1, \Lambda_2, \Lambda_3, \omega_n) = \sqrt{\lambda_1^2}, \quad \beta_{2,n}(\Lambda_1, \Lambda_2, \Lambda_3, \omega_n) = \sqrt{-\lambda_2^2}. \tag{38}$$

Again, in the inverse problem, the resonant frequencies are known; Λ_1, Λ_2 and Λ_3 are unknown. In Eq. (38), $\beta_{1,n}$ and $\beta_{2,n}$ stand for the corresponding β_1 and β_2 values when the known nth resonant frequency of ω_n as an input. Similarly, we define the following function by modifying Eq. (32)

$$\mathcal{G}_n(\Lambda_1, \Lambda_2, \Lambda_3, \omega_n) = 2\beta_{1,n}\beta_{2,n}[1 - \cosh(\beta_{1,n})\cos(\beta_{2,n})] + (\beta_{2,n}^2 - \beta_{1,n}^2)\sinh(\beta_{1,n})\sin(\beta_{2,n}). \tag{39}$$

For a clamped-clamped beam, we set the following parameters of Λ_ns

$$\Lambda_1 = 10^{-2}, \quad \Lambda_2 = -2, \quad \Lambda_3 = 10^{-4}, \tag{40}$$

Compared with those of the hinged-hinged beam in Eq. (34), Λ_1 and Λ_3 keep the same but Λ_2 is quadrupled. Because the buckling load of a clamped-clamped is also quadrupled as $-4\pi^2$ as compared with that of a hinged-hinged beam, this $\Lambda_2 = -2$ value still remains as 5% of the buckling load. With Eq. (40), the first three resonant frequencies of a clamped-clamped beam are solved by Eq. (32) as follows

$$\omega_1 = 21.91442 = (4.68128)^2, \quad \omega_2 = 61.08577 = (7.81574)^2, \quad \omega_3 = 120.08498 = (10.95833)^2. \tag{41}$$

When $\Lambda_1 = \Lambda_2 = \Lambda_3 = 0$, the resonant frequencies of a clamped-clamped beam predicted by the classical theory are the following (Chang and Craig, 1969)

$$\omega_1^o = 22.37329 = (4.73004)^2, \quad \omega_2^o = 61.67282 = (7.8532)^2,$$
$$\omega_3^o = 120.90339 = (10.99561)^2. \tag{42}$$

Compared with ω_n^os of Eq. (42), all three ω_ns in Eq. (41) decreases because of the compression of negative $\Lambda_2 = -2$. If the exact resonant frequencies of Eq. (41) are supplied by an experiment, the following inverse problem formulation is presented for a clamped-clamped beam

$$\begin{cases} \mathcal{G}_1(\Lambda_1, \Lambda_2, \Lambda_3, 21.91442) \\ \quad = 2\beta_{1,1}\beta_{2,1}[1 - \cosh(\beta_{1,1})\cos(\beta_{2,1})] \\ \quad\quad + (\beta_{2,1}^2 - \beta_{1,1}^2)\sinh(\beta_{1,1})\sin(\beta_{2,1}) = 0, \\ \mathcal{G}_2(\Lambda_1, \Lambda_2, \Lambda_3, 61.08577) \\ \quad = 2\beta_{1,2}\beta_{2,2}[1 - \cosh(\beta_{1,2})\cos(\beta_{2,2})] \\ \quad\quad + (\beta_{2,2}^2 - \beta_{1,2}^2)\sinh(\beta_{1,2})\sin(\beta_{2,2}) = 0, \\ \mathcal{G}_3(\Lambda_1, \Lambda_2, \Lambda_3, 120.08498) \\ \quad = 2\beta_{1,3}\beta_{2,3}[1 - \cosh(\beta_{1,3})\cos(\beta_{2,3})] \\ \quad\quad + (\beta_{2,3}^2 - \beta_{1,3}^2)\sinh(\beta_{1,3})\sin(\beta_{2,3}) = 0. \end{cases} \tag{43}$$

Again, three equations for three unknowns of Λ_ns are solved by the Newton-Raphson method. With the exact resonant frequencies supplied, the exact solution of $(\Lambda_1, \Lambda_2, \Lambda_3) = (1 \times 10^{-2}, -2, 1 \times 10^{-4})$ is also obtained.

4. Summary

The effects of strain gradient elasticity, nonlocal elasticity, surface elasticity, surface stress and residual stress can all have impacts on the beam resonant frequencies. Some effects are size-dependent and stand out as the beam dimensions scale down, which are embodied in three dimensionless parameters in this study. In a real application, these three parameters are unknown. The inverse problem of using the shifts of resonant frequencies to determine the three parameters is formulated and solved. The physical mechanisms that the inverse problem can be solved are that the three parameters have different impacts on one resonant frequency and different resonant frequencies respond differently to these three parameters. By solving the three parameters, some effects such as nonlocal elasticity effect can be told; some effects such as surface elasticity and strain gradient elasticity effects are combined into one parameter, which becomes impossible to tell them apart. However, as the beam mechanical properties are characterized by these three parameters, the inverse problem solving method actually provides an effective method to calibrate a micro/nanobeam.

Acknowledgment

The research has been supported by the National Natural Science Foundation of China (NSFC No. 11372321).

References

Abu-Al-Rub, R.K., Voyiadjis, G.Z., 2004. Analytical and experimental determination of the material intrinsic length scale of strain gradient plasticity theory from micro- and nano-indentation experiments. Int. J. Plast. 20, 1139–1182.
Adomeit, G., 1967. Determination of elastic constants of a structured material. In: Kröner, E. (Ed.), Mechanics of Generalized Continua. Springer-Verlag, Stuttgart. IUTAM symposium, Freudenstadt.
Aifantis, E.C., 2003. Update on a class of gradient theories. Mech. Mater. 35, 259–280.
Aifantis, E.C., Willis, J.R., 2005. The role of interfaces in enhancing the yield strength of composites and polycrystals. J. Mech. Phys. Solids 53, 1047–1070.
Altenbach, F., Eremeyev, V.A., 2011. On the shell theory on the nanoscale with surface stresses. Int. J. Eng. Sci. 49, 1294–1301.
Amiot, F., 2013. An Euler-Bernoulli second strain gradient beam theory for cantilever sensors. Philos. Mag. Lett. 93, 204–212.
Anger, G., 1990. Inverse Problems in Differential Equations. Plenum Press, New York.
Arash, B., Wang, Q., 2012. A review on the application of nonlocal elastic models in modeling carbon nanotubes and graphene. Comput. Mater. Sci. 51, 303–313.
Boisen, A., 2009. Mass spec goes nanomechanical. Nature Nanotech. 4, 404–405.
Chajes, A., 1974. Principles of Structural Stability Theory. Prentice-Hall, Inc., Englewood Cliffs, New Jersey.
Chang, T.C., Craig, R. R., 1969. Normal modes of uniform beams. J. Eng. Mech. 195, 1027–1031.
Cosserat, E., Cosserat, F., 1909. Theorie des Corps Deformables. A. Hermann et Fils, Paris.
Dillard, T., Forest, S., Ienny, P., 2006. Micromorphic continuum modelling of the deformation and fracture behavior of nickel foams. Eur. J. Mech. A/Solids 25, 526–549.
Ellis, R.W., Smith, C.W., 1966. A thin-plate analysis and experimental evaluation of couple-stress effects. Exp. Mech. 7, 372–380.
Eringen, A.C., 1983. On differential equations of nonlocal elasticity and solutions of screw dislocation and surface waves. J. Appl. Phys. 54, 4703–4710.
Eringen, A.C., 1968. Theory of micropolar elasticity. In: Liebowitz, H. (Ed.), Fracture, Vol. 2. Academic, New York, pp. 621–729.
Fleck, N.A., Willis, J.R., 2015. Strain gradient plasticity: energetic or dissipative? Acta Mech. Sin. 31, 465–472.
Forest, S., 2009. Micromorphic approach for gradient elasticity, viscoplasticity, and damage. J. Eng. Mech. 135, 117–131.
Forest, S., Sievert, R., 2006. Nonlinear microstrain theories. Int. J. Solids Struct. 43, 7224–7245.
Gauthier, R.D., Jahsman, W.E., 1975. A quest for micropolar elastic constants. J. Appl. Mech. 42, 369–374.
Gladwell, G.M.L., 2004. Inverse Problems in Vibration, 2nd edition Kluwer Academic Publisher, New York.
He, J., Lilley, C.M., 2008. Surface stress effect on bending resonance of nanowires with different boundary condition. Appl. Phys. Lett. 93, 263108.
Kakunai, S., Masaki, J., Kuroda, R., Iwata, K., Nagata, R., 1985. Measurement of apparent Young's modulus in the bending of cantilever beam by heterodyne holographic interferometry. Exp. Mech. 25, 408–412.
Karabalin, R.B., Villanieva, L.G., Matheny, M.H., Sader, J.E., Roukes, M.L., 2012. Stress-induced variations in the stiffness of micro-and nanocantilever beams. Phys. Rev. Lett. 108, 23610.
Koiter, W.T., 1964. Couple-stresses in the theory of elasticity I and II. Koninkl. Ned. Akad. Wet. Ser. B 67, 17–44.
Kong, S., Zhou, S., Nie, Z., Wang, K., 2008. The size-dependent natural frequency of Bernoulli-Euler micro-beams. Int. J. Eng. Sci. 46, 427–437.
Kong, S., Zhou, S., Nie, Z., Wang, K., 2009. Static and dynamic analysis of micro beams based on strain gradient elasticity theory. Int. J. Eng. Sci. 47, 487–498.
Kröner, E., 1963. On the physical reality of torque stresses in continuum mechanics. Int. J. Eng. Sci. 1, 261–278.
Lakes, R.S., 1986. Experimental microelasticity of two porous solids. Int. J. Solids Struct. 22, 55–63.
Maranganti, R., Sharma, P., 2007a. Length scales at which classical elasticity breaks down for various materials. Phys. Rev. Lett. 98, 195504.
Maranganti, R., Sharma, P., 2007b. A novel atomistic approach to determine strain–gradient elasticity constants: tabulation and comparison for various metals, semiconductors, silica, polymers and the (Ir) relevance for nanotechnologies. J. Mech. Phys. Solids 55, 1823–1852.
McFarland, A.W., Colton, J.S., 2005. Role of material microstructure in plate stiffness with relevance to microcantilever sensors. J. Micromech. Microeng. 15, 1060–1067.
Mindlin, R.D., 1963. Influence of couple-stresses on stress concentrations. Exp. Mech. 3, 1–7.
Mindlin, R.D., 1964. Micro-structure in linear elasticity. Arch. Rat. Mech. Anal. 16, 51–78.
Mindlin, R.D., 1972. Elasticity, piezoelectricity and crystal dynamics. J. Elast. 2, 217–282.
Mindlin, R.D., Eshel, N.N., 1968. On first strain-gradient theories in linear elasticity. Int. J. Solids Struct. 4, 109–124.
Mindlin, R.D., Tiersten, H.F., 1962. Effects of couple-stresses in linear elasticity. Arch. Rat. Mech. Anal. 11, 415–448.
Murphy, K.D., Zhang, Y., 2000. Vibration and stability of a cracked translating beam. J. Sound Vib. 237, 319–335.
Perkins, R.W., Thompson, D., 1973. Experimental evidence of a couple-stress effect. AIAA J. 11, 1053–1055.
Press, W.H., Teukolsky, S.A., Vetterling, W.T., Flannery, B.P., 1992. Numerical Recipes in Fortran, 2nd edition Cambridge University Press, Cambridge.
Reed, J., Wilkinson, P., Schmit, J., Klug, W., Gimzewski, J.K., 2009. Observation of nanoscale dynamics in cantilever sensor arrays. Nanotechnology 20, 395707.
Schijve, J., 1966. Note on couple stresses. J. Mech. Phys. Solids 14, 113–120.
Wang, L., Hu, H., 2005. Flexural wave propagation in single-walled carbon nanotubes. Phys. Rev. B 71, 195412.
Wu, J., Wei, Y., 2013. Grain misorientation and grain-boundary rotation dependent mechanical properties in polycrystalline graphene. J. Mech. Phys. Solids 61, 1421–1432.
Xu, M., 2006. Free transverse vibrations of nano-to-micron scale beams. Proc. R. Soc. A 462. 2977–2955.
Yang, J., Lakes, R.S., 1981. Transient study of couple stress effects in compact bone: torsion. J. Biomech. Eng. 103, 275–279.
Yang, J., Lakes, R.S., 1982. Experimental study of micropolar and couple stress elasticity in compact bone in bending. J. Biomech. 15, 91–98.

Zhang, G., Gao, X.L., Wang, J., 2015. A non-classical model for circular Kirchhoff plates incorporating microstructure and surface energy effects. Acta Mech. 226, 4073–4085.
Zhang, Y., 2013. Determining the adsorption-induced surface stress and mass by measuring the shifts of resonant frequencies. Sens. Actuators A 194, 169–175.
Zhang, Y., Zhao, Y.P., 2014. Detecting the mass and position of an adsorbate on a drum resonator. Proc. R. Soc. A 470, 20140418.
Zhang, Y., Zhao, Y.P., 2015. Determining both adhesion energy and residual stress by measuring the stiction shape of a microbeam. Microsyst. Technol. 21, 919–929.
Zhang, Y., Zhuo, L., Zhao, H., 2013. Determining the effects of surface elasticity and surface stress by measuring the shifts of resonant frequencies. Proc. R. Soc. A 469, 20130449.
Zhang, Y.Q., Liu, G.R., Xie, X.Y., 2005. Free transverse vibration of double-walled carbon nanotubes using a theory of nonlocal elasticity. Phys. Rev. B 71, 195404.
Zhang, Y.Y., Wang, C.M., Challamel, N., 2010. Bending, buckling, and vibration of micro/nanobeams by hybrid nonlocal model. J. Eng. Mech. 136, 562–574.
Zhang, Y.Y., Wang, C.M., Duan, W.H., Xiang, Y., Zong, Z., 2009. Assessments of continuum mechanics models in predicting buckling strains of singe-walled carbon nanotubes. Nanotechnology 20, 395707.